FATIGUE LIFE PREDICTION OF INJECTION MOLDED SHORT GLASS FIBER REINFORCED PLASTICS

Marc J.W. Kanters, Lucien F.A. Douven
DSM Materials Science Center, Geleen, The Netherlands
Pierre Savoyat
e-Xstream engineering, Brussels, Belgium

Abstract

This work presents a framework that combines experimental and numerical methods to achieve accurate prediction of the fatigue life of short fiber reinforced parts. The framework combines engineering tools that allow design engineers to predict fatigue life of engineering plastics applications, including anisotropy in high detail. The framework involves characterization of the proper failure mechanisms, modelling of anisotropy, and compensation for local stress concentrations. This paper highlights the key features of the framework and demonstrates and validates its predictability on a representative demonstration part.

Introduction

Thermoplastic composites, where continuous or short fibers are embedded in a thermoplastic matrix, are increasingly used in a large range of applications. These materials can offer weight reduction via metal to plastic conversion [1]. With industry striving to reduce weight even further [2,3], the upcoming trend is to also realize load bearing structural parts in reinforced plastics [1,4].

To prevent premature failure in service, predictability is key when designing load bearing components. This work focusses on fatigue lifetime predictions of injection molded short glass fiber reinforced plastics (SFRP).

The first step to accurately predict lifetime of SFRP's is to properly understand and model the mechanisms that lead to long-term failure. In general, for thermoplastics one can distinguish three failure mechanisms: i) plasticity-controlled failure, related to creep or accumulation of plastic strain, ii) slow crack growth, controlled by gradual crack propagation, and iii) molecular degradation [5,6]. With all three having a different origin, each is affected differently by loading conditions, such as load magnitude, load amplitude or load ratio, and frequency [7-9]. This work focusses on the first two failure mechanisms.

The second step is to capture the anisotropic material behavior, induced by the local glass fiber orientation caused by the injection molding process. The local alignment of fibers can easily induce variations in stiffness and strength of a factor of 1.5 to 2 [10]. Hence, one needs to accurately capture the local glass fiber orientation after processing and properly model the resulting anisotropic material behavior. Unfortunately, modelling the correct failure mechanisms and anisotropy is not enough and improvement requires including more features, such as local stresses, stress gradients, and local load ratios.

This work presents the results of an effort to improve the accuracy of fatigue life predictions via a step-by-step approach where the complexity in loading conditions, anisotropy, and stress state is increased systematically. The resulting framework combines engineering tools, enabling

design engineers to predict fatigue lifetime of engineering plastics applications in an efficient workflow. Key features are highlighted, and the framework is demonstrated and discussed on a representative demonstrator part.

Experimental section

Materials and geometries

The material used was a polyamide 66 reinforced with 50wt.% of glass fibers, from which tensile specimens (ASTM D638 Type S) and plaques with dimensions of 270x310x2mm are molded. From the plaques, tensile specimens (ISO527 1B and ASTM D638 Type S) were milled (one per plate) at various angles with respect to the flow direction, whilst their center was always at the same position in the plaque where the flow front was fully evolved. Double edge notched specimens are machined from the ISO527 1B tensile bars with various radii to study the sensitivity for stress concentrations. An in-house developed DSM demonstrator part was molded and tested in the same material.

Mechanical testing

Fatigue experiments were performed on a servo-hydraulic MTS Testing System equipped with a 25kN load cell. During all load controlled cyclic fatigue experiments, a sinusoidal stress was applied up to failure. The maximum load, load ratio, defined as $R = \sigma_{min}/\sigma_{max}$, and frequency were kept constant during each experiment. Frequency was 0.25Hz for the test specimens and 1Hz for the demonstrator part. A wide range of load ratios was used; load levels were selected to obtain fatigue lives between 10^2 and 10^6 cycles.

Microstructure

During the injection molding process of glass fiber reinforced materials, the glass fibers align, and a specific microstructure will result for each sample type. The glass fiber orientation for the two geometries used (the injection molded Type S bar and the plate), quantified using X-ray microtomography, are presented in Figure 1. The measurement is done on a small sample cut from the center of the injection molded tensile bar and the location in the plate that corresponds to the center of the milled tensile specimens. The injection molded Type S bars display a strong, homogenous orientation over the sample thickness, caused by a plug flow in the narrow section. The plate specimens display a distinct shell/core type of morphology due to the expansion flow in the core and the shear flow at the walls of the cavity.

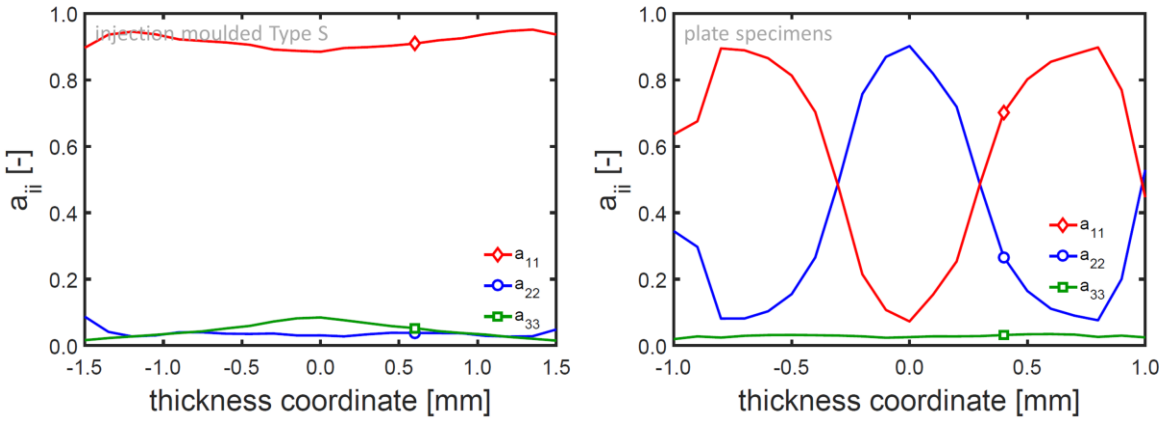

Figure 1: Glass fiber orientation for the injection molded Type S tensile bar (left) and the plate specimens (right). a_{11} represents orientation in flow direction, a_{22} in-plane and perpendicular to the flow direction, and a_{33} out-of-plane.

Material model calibration

Numerical methods

For modelling of the mechanical performance of short glass fiber reinforced plastics (SFRP) an integrative approach is developed, where the effects of the injection molding process are included. This combines multiple software tools: I) injection molding simulation software to predict the orientation of the glass fibers (Autodesk Moldflow, version 2019), II) material modelling software tools (Digimat, version 2019.0), III) a FE code (Abaqus, version 2018) to simulate the mechanical part performance, and IV) an interface to compute lifetime, as illustrated by Figure 2.

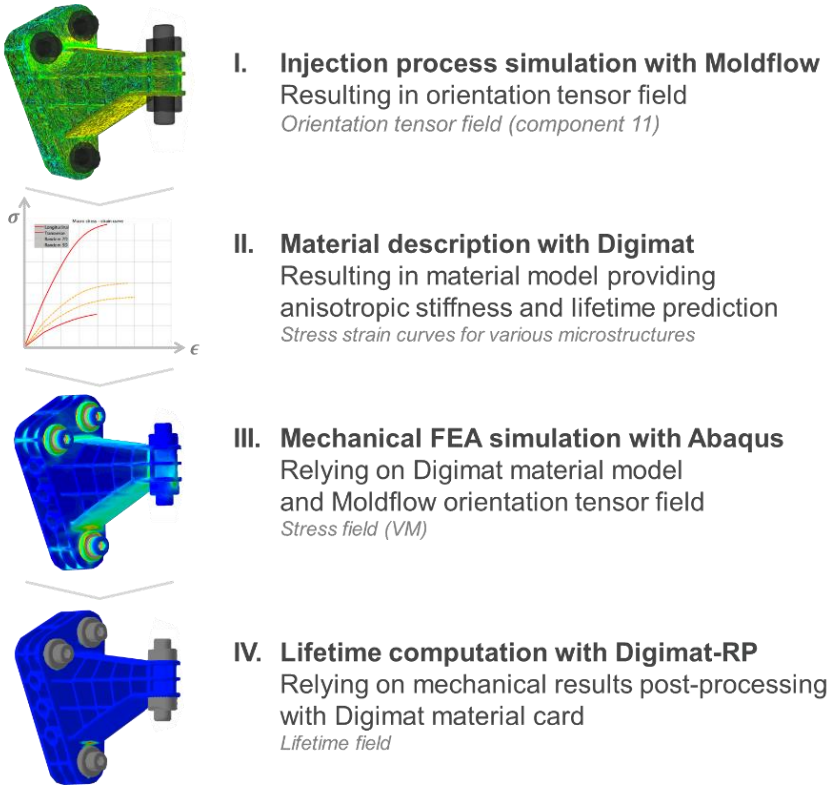

Figure 2: Overview of the numerical workflow.

The material modelling software package Digimat can efficiently and accurately model the influence of glass fiber orientation on mechanical properties, where the complex heterogeneous microstructure is represented by pseudo-grains and homogenized using mean-field theory to define the representation by an equivalent homogenous one. For more details, see [11]. For the used workflow, Digimat also maps the glass fiber orientation from the Moldflow mesh to the Abaqus mesh, calibrates the material model, provides an interface for that material model to the FE code (Abaqus), and performs lifetime calculations.

The Digimat material model for lifetime prediction is calibrated in three steps, as illustrated in Figure 3: I) the calibration of an elastic model capturing anisotropic stiffness for any microstructure, II) the calibration of a fatigue model to predict lifetime for any microstructure, stress amplitude and load ratio, and III) the enrichment of the model lifetime prediction via the calibration of post-processing parameters capturing the sensitivity to stress concentration.

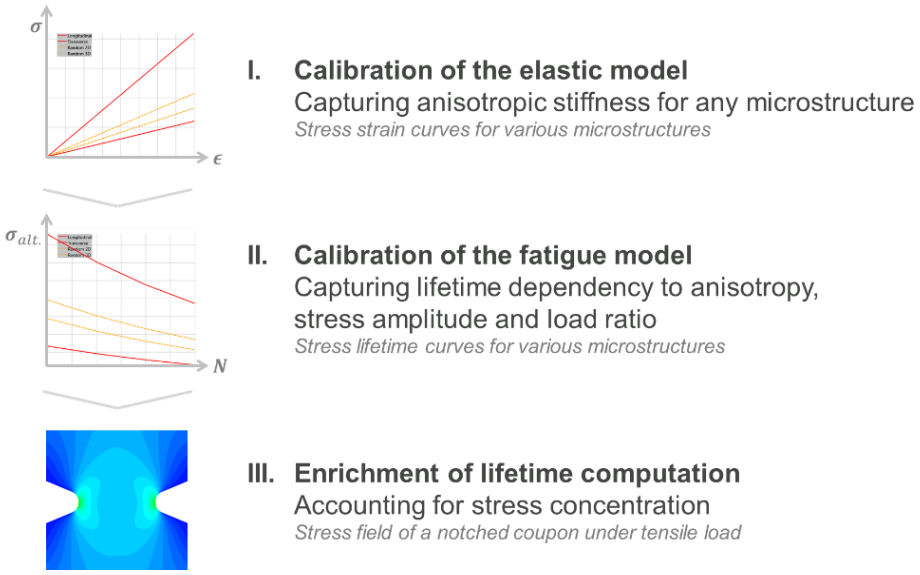

Figure 3: Overview of the workflow for material model calibration within Digimat

Anisotropic stress-strain response

To compute the stress field used to calculate lifetime, an anisotropic linear elastic material model is used, calibrated on the stiffness measured on specimens milled at various orientations from an injection molded plate. Full calibration requires the material's microstructure (glass fiber content, effective glass fiber aspect ratio, and the glass fiber orientation distribution from the micro-CT data, see Figure 1), and the glass fiber properties (Young's modulus, Poisson's ratio and density). Using these, the material model can be completed by fitting the linear elastic properties of the thermoplastic polymer matrix. The microstructure was modelled in high detail (21 elements or layers over the sample thickness) to properly capture the distinct shell-core structure, and model prediction and experimental results are compared in Figure 4.

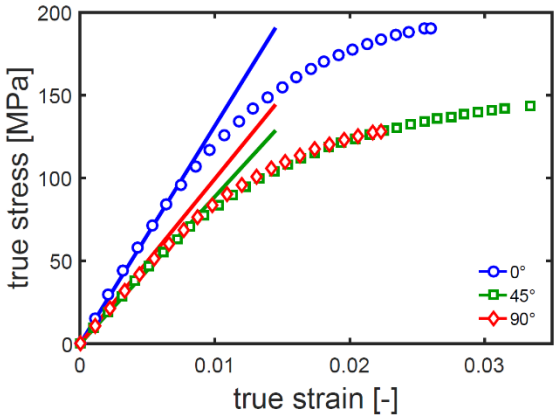

Figure 4: Stress-strain curves for the plate specimens taken at 0°, 45° and 90° (markers), compared with the model fits (lines, only stiffness)

Localization factor K_t

During experimental material characterization, force and displacement are recorded and subsequently converted to nominal stress and strain. For fiber reinforced materials, stress and strain often localizes in specific regions of the test specimen and, naturally, the local values will deviate from the nominal. Since in the FE analyses the local values are computed, this must be considered to ensure consistency between experiment and simulation.

To efficiently do so, a localization factor, K_t, is used that transforms the macroscopic nominal stress values to local values. The stress-based localization factor is defined as the ratio between the local stress at the hot spot and the nominal stress in the experiment. Its magnitude is computed for each fatigue load case and is used to scale the SN-curves from nominal to local, before calibrating the final fatigue model, as displayed in Figure 5.

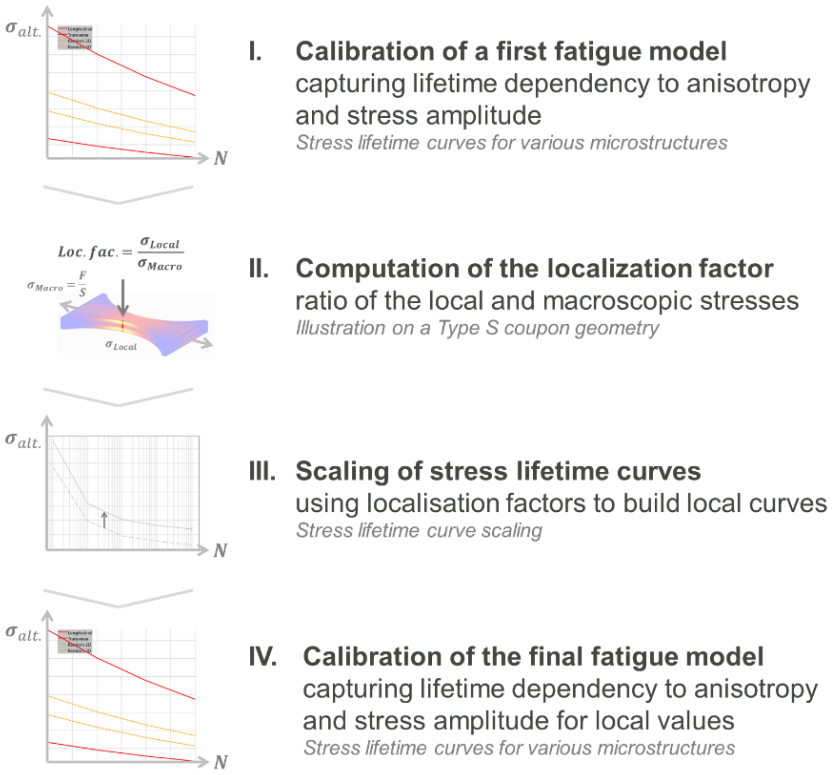

Figure 5: Illustration of the workflow to correct for the localization factor

Fatigue failure model: Load ratio and anisotropy

The influence of load ratio, R, was studied using molded tensile bars, and the influence of anisotropy was studied using samples taken from the plate machined under various angles with respect to the flow direction. The SN-curves that resulted are presented in Figure 6.

Figure 6a shows that there are two distinct failure mechanisms for these load ratios at this temperature and on these timescales. At $R = 1$, plasticity-controlled failure (small slope) is observed and at all the other load ratios failure is dominated by crack-growth controlled failure (large slope). Both failure mechanisms were modelled using analytical models, for more details see [8,9], resulting in the solid lines in Figure 6a.

Figure 6b compares experiments with the analytical models (solid lines) for various samples with different microstructures. The Digimat material model, based on Tsai-Hill failure indicators, is calibrated using the 21 layered microstructure and these model fits, whilst considering the localization factor K_t. The dashed lines in Figure 6a and b show that the influence of mean stress and anisotropy is properly captured by the Digimat material model.

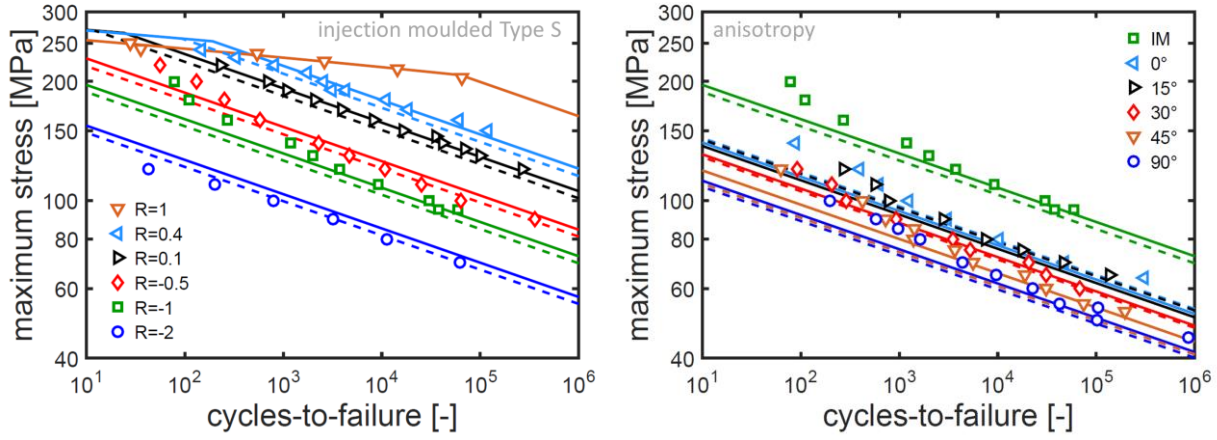

Figure 6: SN-curves for injection molded tensile bars at various load ratios (a) and for various microstructures at $R = -1$ (b). Markers represent measurements, solid lines the analytical model, dashed lines the Digimat material model.

To further validate the calibrated material model, the predicted lifetime for various load ratios for samples taken under 0° and 90° orientation are compared to the experimental values in Figure 7a, showing the Digimat material model accurately describes the influence of both microstructure and load ratio. To underline the overall consistency, a comparison with all the experimental results on tensile specimens is presented in Figure 7b, showing a very satisfying agreement between model and experiments. Furthermore, it shows that, even for this relatively simple geometry, the accuracy that can be expected capturing load ratio and anisotropy is easily exceeding ± factor 3, originating from the fitting compromises on both the analytical and the Digimat material model.

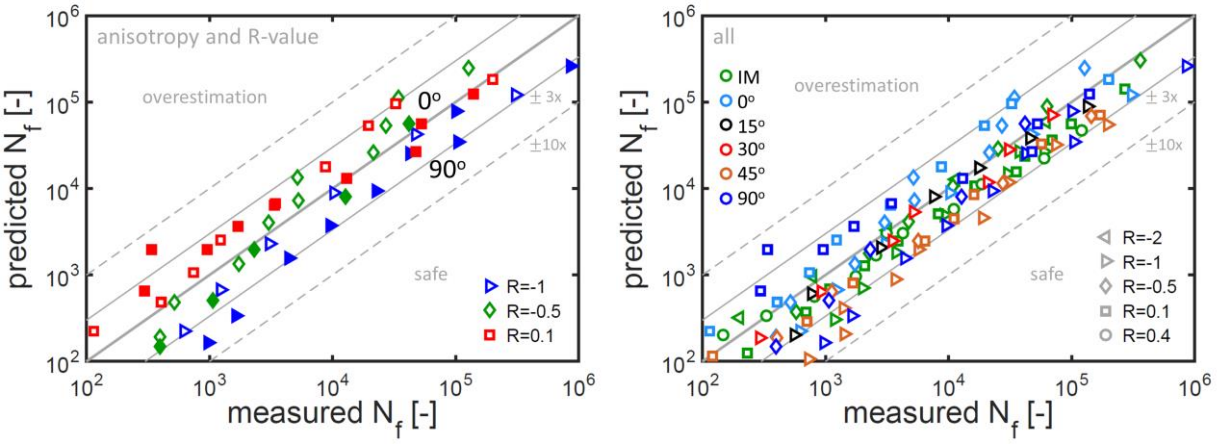

Figure 7: (a) Comparison of the model and experiments for samples with 0° (open markers) and 90° (solid markers) orientations for different R-values. (b) Comparison of the model and experiments and all the specimen data, where different marker types represent different load ratios and colors the various orientations.

Fatigue failure model: Stress concentrations

From various studies on metals it is well-known that for accurate lifetime predictions it is necessary to compensate for local stress concentrations, and the same methods are applied to model plastics [12-14]. Here we will demonstrate the approach while using the theory of critical distances [15].

To account for a local stress concentration, the magnitude of the local stress, σ_{local}, is scaled down using the fatigue notch factor, K_f, to obtain an effective stress to use for lifetime calculation, σ_{eff}, via:

$$\sigma_{eff} = \frac{\sigma_{local}}{K_f} \tag{1}$$

To obtain a value for K_f, the lifetime is computed using the local stress and the resulting lifetime is compared with the experimental value. Via the stress dependency of the SN curve the value for K_f can be computed that would allow to match the experimental results. Preferably, multiple load levels are used and an average K_f is determined by shifting the entire computed SN curve over multiple experiments.

To define K_f for any arbitrary stress concentration, the theory of critical distances is used. This relates the normalized stress gradient, χ, to K_f by the characteristic length, ρ^*, via:

$$\chi = \frac{1}{\sigma_{max}}\frac{d\sigma}{dx} \quad \text{and} \quad K_f = 1 + \sqrt{\chi \cdot \rho^*} \tag{2}$$

Here we use the path perpendicular to the maximum principal stress to compute the 1-D stress gradient.

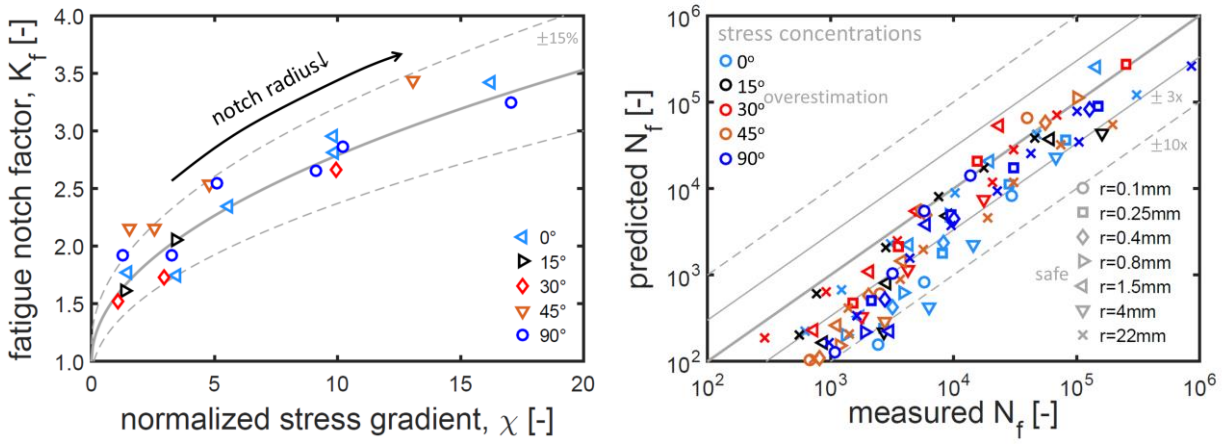

Figure 8: K_f versus χ for different notch radii and sample orientations (a). Comparison of the Digimat material model and experiments for specimens with different notch radii at $R = -1$, where different markers represent different notch radii, different colors the different sample orientations (b).

Figure 8a summarizes the dependence of the fatigue notch factor K_f on the normalized gradient χ. Assuming the characteristic length is independent of fiber orientation and fitting a single value for ρ^* on this dataset (Figure 8a, gray lines) describes K_f within ±15% accuracy for this wide range of stress gradients. Please be aware that the scaling of the local stress with ±15% accuracy can easily introduce ± factor 5 error in lifetime.

In this case also the test geometry used for the characterization of the material card comprises a minor gradient in stress, and therefore, to remain consistency between model and experiments for all the different geometries, the material model requires recalibration. Like the procedure to consider the localization factor K_t (see Figure 5), this is done by rescaling the input curves using the K_f for that specific geometry. However, it is important to realize that because this also affects the predictions for the notched specimens, proper calibration requires an iterative loop of scaling the input curves, and re-computing the experimental K_f and corresponding characteristic length.

Once properly done, the model will provide consistent results. This is displayed in Figure 8b for a range of notch radii, where results for $r = 22mm$ representing the Type S geometry are included. There is a very good agreement between model and experiments for the higher number of cycles for a large range of notch radii. At shorter number of cycles there appears to be a systematic underestimation by the model, related to the use of the linear elastic material model. We believe this can be solved by using an elastoplastic material model or via a plasticity correction according to e.g. Neuber or Glinka's approach [16,17]. The latter is currently being implemented within the Digimat software and first results indeed suggest additional accuracy.

Material model validation

The material model calibrated in the previous section is validated on an in-house developed demonstrator part that is injection molded in the same material and tested in fatigue for different load ratios. To predict the fatigue lifetime, the workflow presented in Figure 2 is used and this section presents the results of the different steps taken.

Fiber orientation from processing simulation

Moldflow is used to predict the local fiber orientation. To improve the accuracy of the material model used in the processing simulation, first the processing simulation of the 2 mm plates is performed. The resulting prediction for the fiber orientation is compared to the experimental results in Figure 1, and the parameters of the fiber orientation model are adjusted until both agree well. With these parameters, the processing simulation on the demonstrator part is performed. To validate the accuracy of the flow simulation, a section nearby the failure location is taken from the demonstrator part, the area highlighted in Figure 9, where the fiber orientation is characterized by X-ray microtomography. The predicted and measured fiber orientations are compared in Figure 9, showing that nearby the failure location (x=0) the predicted values match the experimental ones very well. So, although there is still room for improvement for the model to predict the orientation towards the middle of the sample, the comparison shows the computed fiber orientation can be used to calculate the stresses and lifetimes in the critical location of the demonstrator part.

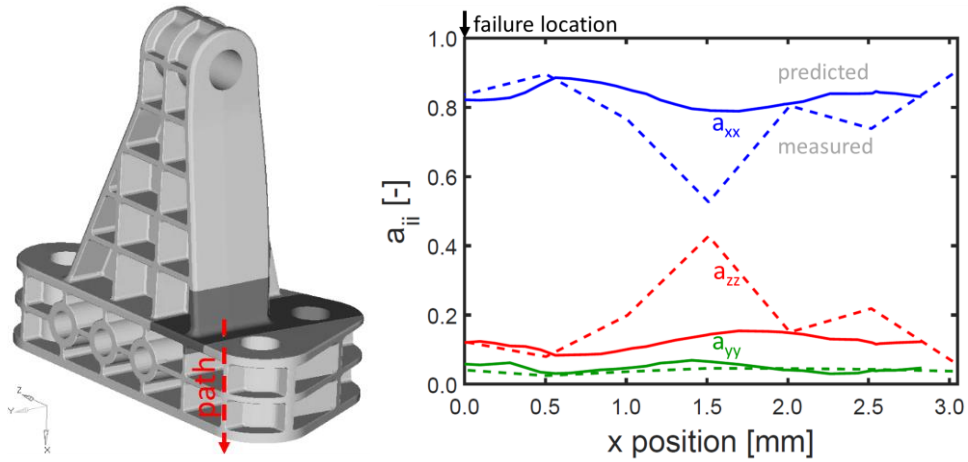

Figure 9: Left: The demonstrator part, where the darker area represents the section cut to measure the fiber orientation using X-ray microtomography. Right: The fiber orientation prediction from Moldflow (solid lines) and the experimental values (dashed lines). The arrow on the left graph indicates the direction represented on the x-axis in the graph and x=0 is nearby the failure location, the total path of 3 mm only considers the top flange.

Stress computations: Local stress ratio

As can be observed in Figure 9 and Figure 11a, the demonstrator part is asymmetric, hence so is the structural stiffness of the part. Consequently, the local stresses that result from a macroscopic force will differ when the part is loaded in tension or compression. This is illustrated in Figure 10 showing that loading the demonstrator part with 1500N results in a local maximum principal stress at the failure location of 94.3MPa. When reversing a load with the same magnitude, the resulting minimum principal stress at the failure location is -34.3MPa. So, while the force ratio, R_F, equals -1, the local stress ratio, R_σ, is only -0.36. On top of the geometrical asymmetry, the boundary conditions can also affect the local stress state. For example, the demonstrator part is mounted to the fixture by bolts and washers, as can be seen in Figure 12a. These are included in the FEA model and influence R_σ, since the bolt pretension exerts a small tensile load in the critical location.

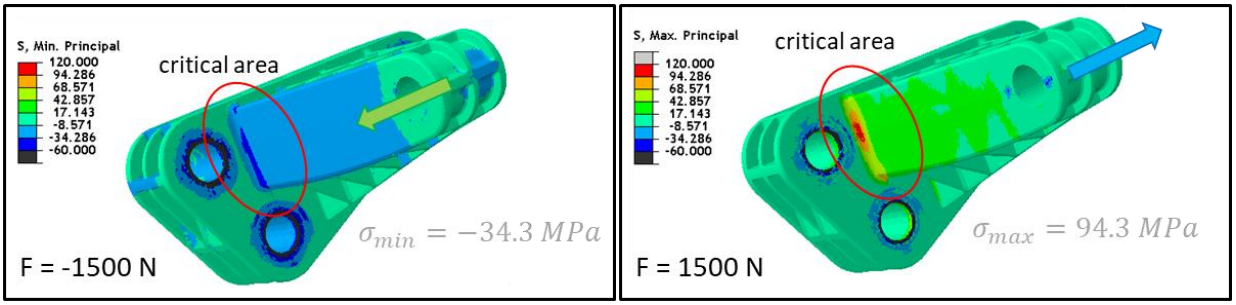

Figure 10: Local stresses in the failure location of the demonstrator part loaded in with a minimum load of -1500N (a) and a maximum load of 1500N (b).

Figure 10 shows how the local stress ratio varies as function of the maximum applied force, highlighting how large the variations can be between R_F and R_σ. For example, for $R_F = -1$ the value of R_σ varies from 0.08 to -0.53 within a maximum applied force range of 0 - 3 kN. And, as Figure 6a already shows, the variations in lifetime can be easily in the order of a factor 5 to 100, clearly showing the necessity of considering the local stress ratio, instead of assuming a (constant) ratio equal to the macroscopically applied ratio.

The Digimat software allows to do this via three different routes: 1) Manually determine the local magnitudes of principal stresses at the maximum and minimum load to manually compute R_σ and let the software compute lifetime using that value, 2) Use two load cases with opposite directions, define the increments of interest that correspond to a macroscopic load and R_F, after which the software computes R_σ and the resulting lifetime, or 3) Use a load case that simulates one load cycle, and allows the software to determine the minimum and maximum stress levels, the value of R_σ, and the lifetime.

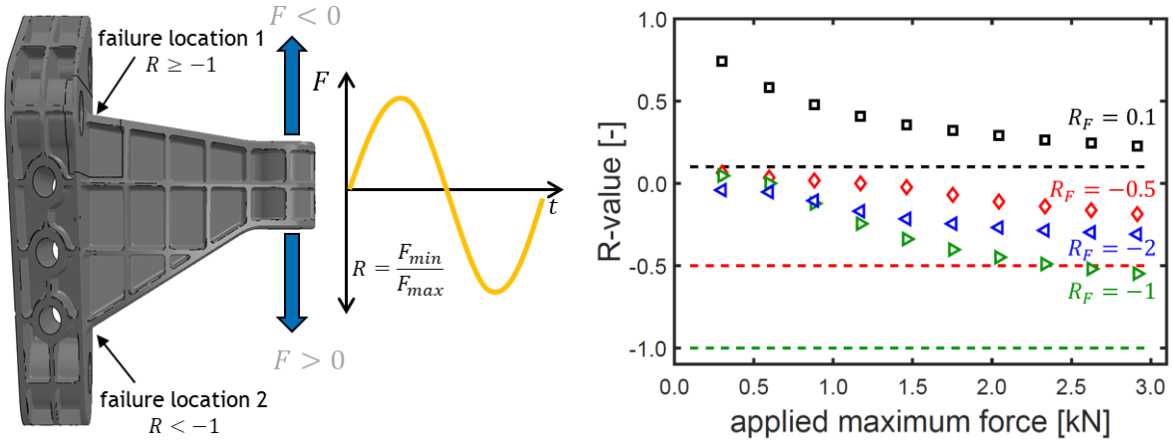

Figure 11: (a) Model of the demonstrator part, illustrating the loading directions and two failure locations, depending on the load ratio. (b) R-value as function of applied load for the demonstrator part, where markers represent the local stress ratio, R_σ, and the dashed lines the macroscopically applied force ratio, R_F.

Lifetime predictions for the demonstrator part

By properly capturing the influence of local stress, fiber orientation, stress concentration, and local stress ratio, the lifetime computations can be performed for the demonstrator part.

Identifying failure locations

For the range of load ratios applied, it could experimentally be observed that the for $R_F \geq -1$ failure occurred by crack formation at the top of the demonstrator part (failure location 1 in Figure 11a). For smaller values of R_F, the cracks formed at the bottom (failure location 2 in Figure 11a). So, the first prerequisite of an accurate lifetime prediction is to properly identify the critical location. To illustrate this, the minimum lifetime in an element set located at the top is (highlighted in orange in Figure 12a) compared with the minimum lifetime in an element set at the bottom (highlighted in green in Figure 12b). The results, before correcting for the stress gradient, are summarized in Figure 12b, showing that indeed for $R_F \geq -1$ lifetime is lowest at the top side (location 1) and for $R_F = -2$ the lifetime is lowest at the bottom side (location 2), confirming the framework accurately identifies the critical failure location.

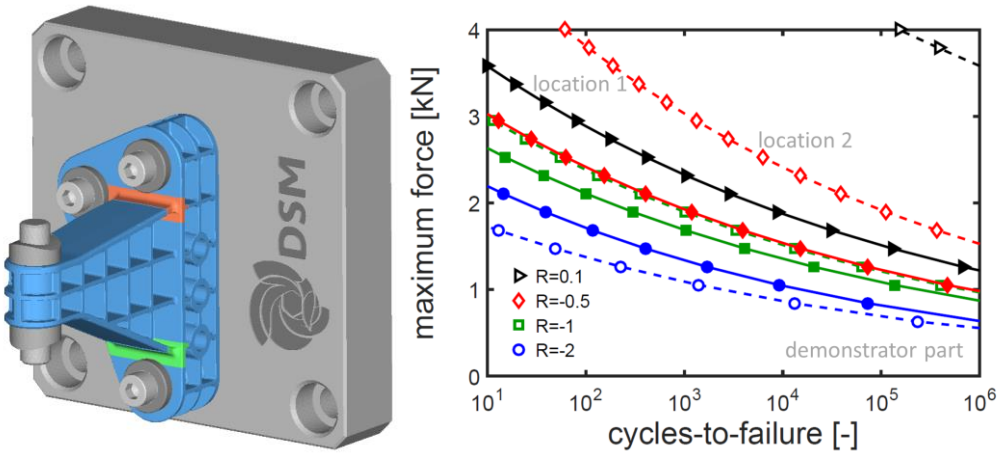

Figure 12: (a) The load case used in the simulation, highlighting the two element sets for failure at the top (failure location 1) highlighted in orange and for failure at the bottom (failure location 2) highlighted in green. (b) Predicted FN curves for failure location 1 and failure location 2 of the demonstrator part at different values for R_F, without gradient correction. Solid lines and closed markers represent the minimum lifetime at the top (location 1), dashed lines and open markers the minimum lifetime at the bottom (location 2).

Prediction accuracy

The accuracy of the framework is shown by comparing the model predictions with the experimental results. To emphasize the need for a proper gradient correction, a model calibrated by including local stress, fiber orientation and local stress ratio, but without recalibration and correction for the stress concentrations is compared to the final model that does consider the stress concentrations. The results are summarized in Figure 13. Figure 13a shows the comparison of the fatigue curves, displaying that both models are conservative. However, where the prediction without correction for stress concentration is approximately a factor 200 conservative, the final model based on the systematic approach using the normalized stress gradient improves the accuracy with more than a factor 20. When summarizing the data also for

the other load ratios, see Figure 13b, it highlights that the overall accuracy of a model without correction is a factor 100-1000 conservative and the systematic approach with gradient correction a factor 5-30. It also shows the dependence on both force ratio and maximum force is captured very well, supported by the slope close to 1 in the predicted versus measured lifetime plot and the overlap for different force ratios. This suggests that the model captures the stress dependency and influence of (local) stress ratio properly, but there is a mismatch in absolute stress level, and the deviations are merely a consistent offset.

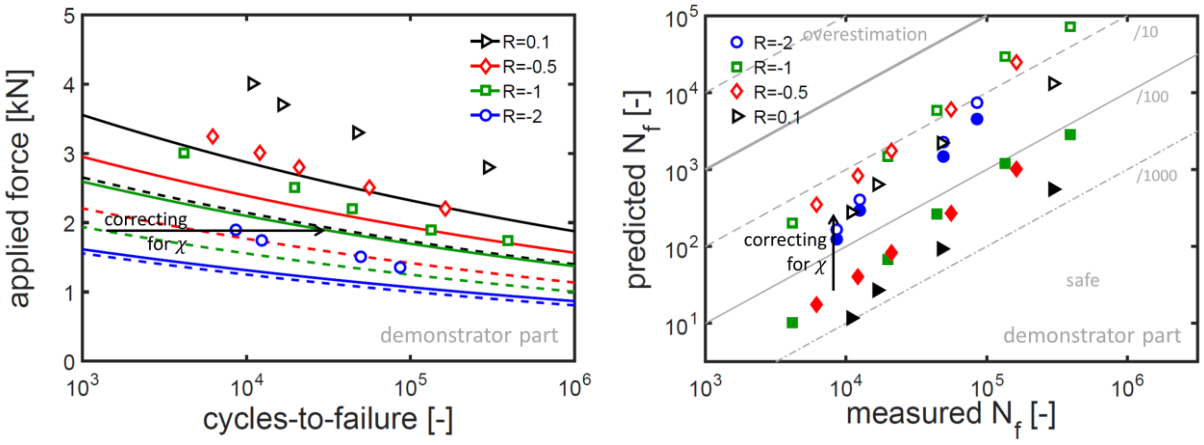

Figure 13: (a) FN curves for the demonstrator part, comparing the model predictions without (dashed lines) and with stress concentration correction methods (solid lines) against measured values (markers). (b) Comparison of the Digimat material model lifetime predictions and experimental lifetimes for the demonstrator part. Solid markers represent the accuracy of a material model by systematically adding complexity, but without inclusion of the stress concentration correction, open markers represent the accuracy of the model that does.

Although the error of a factor 5-30 might seem large, it is already considered as a step-up on overall predictability keeping in mind the large range of variables that are being captured. Furthermore, it is important to realize that the origin of the deviations is clear. For example, as already was shown in Figure 8, the stress concentration correction via the theory of critical distances captures the sensitivity for gradients with an accuracy of ±15% on K_f or a factor 5 in lifetime. Alternative correction methods are investigated for improved predictions in ongoing work. Additionally, besides the choice of correction method, the calibration of the correction method is not optimal. The normalized stress gradient in the demonstrator part is only 0.64 (the radius of the fillet where the failure initiates is 2.5 mm), which is well below the large and ambitious range of normalized stress gradients used to determine the characteristic length. So instead of using a model that is consistent in accuracy for a large range of geometries, it might be preferred to tailor the calibration on ranges relevant for the final geometry. For example, determine the value for the characteristic length on a specimen with comparable stress gradient as the application, or use prior knowledge on part level to determine a value for the characteristic length suitable to that specific geometry. The latter would require a single measurement on part level and would allow accurate prediction of the lifetime for any arbitrary load ratio and applied maximum force and has an even higher accuracy. This is demonstrated in Figure 14a, where the initial prediction is used to determine the suitable K_f value for the demonstrator part, which is subsequently used to correct all other predictions as well, summarized in Figure 14b, showing an accuracy well within $\pm$ factor 4 for all force ratios and applied forces.

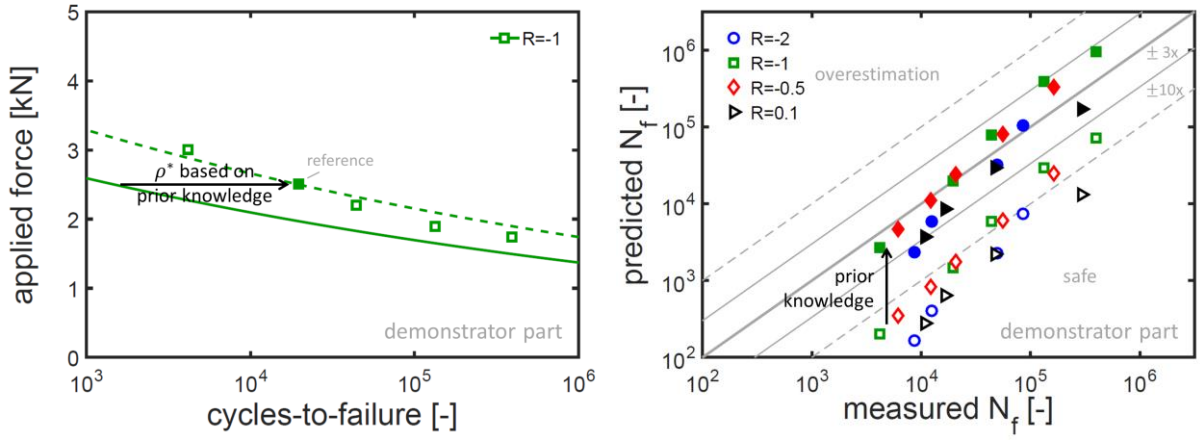

Figure 14: (a) FN curves for the demonstrator part at R_F=-1, illustrating the calibration for the stress concentration correction (via the characteristic length ρ^*) based on prior knowledge. Lines represent the model predictions, markers experimental results, the solid marker the experiment used for calibration. b) Comparison of the Digimat material model lifetime predictions and experimental lifetimes for the demonstrator part for various force ratios. Open markers represent the accuracy of the systematic material model consistent for all geometries, solid markers that of a material model where the stress concentration correction is tailored on the application using prior knowledge.

Dependence on mesh size

Previous results were obtained using a relatively fine mesh at the failure location (element size of 0.1 mm). To investigate the sensitivity of the lifetime computation for mesh size, also simulations are performed with a coarser mesh (element size of 0.5 mm) at the failure location. The resulting predictions of the fatigue lifetime for $R = -1, 0.1$ and 0.5 are provided in Figure 15a, showing the fine mesh provides lifetimes that are approximately a factor two larger for all cases.

This might seem counter intuitive, since one would reasonably expect lower lifetimes for a finer mesh as a higher mesh density usually result in higher local stresses. However, it is important to realize that the mesh density also affects the stress gradient. With increasing mesh density, both the local stress and the normalized stress gradient increase. As a result, the corrected lifetime is only affected to a very limited extend. This is highlighted in Figure 15b, which shows that the uncorrected lifetime for the coarse mesh is 1.7 times higher than for the fine mesh, suggesting a local stress in the coarse mesh of approximately 5% lower than in the fine mesh. However, since the normalized stress gradient in the coarse mesh is much smaller, only 0.38 compared to 0.64 for the fine mesh, the magnitude of K_f is much smaller, and the observed trend for the lifetime after correction is opposite. For guidance in which mesh size is required a more sophisticated study is required, analyzing how the maximum stress and gradient evolves with mesh density and when the value for K_f converges. However, with the overall accuracy this shows that both mesh sizes presented here are sufficiently dense for proper predictions.

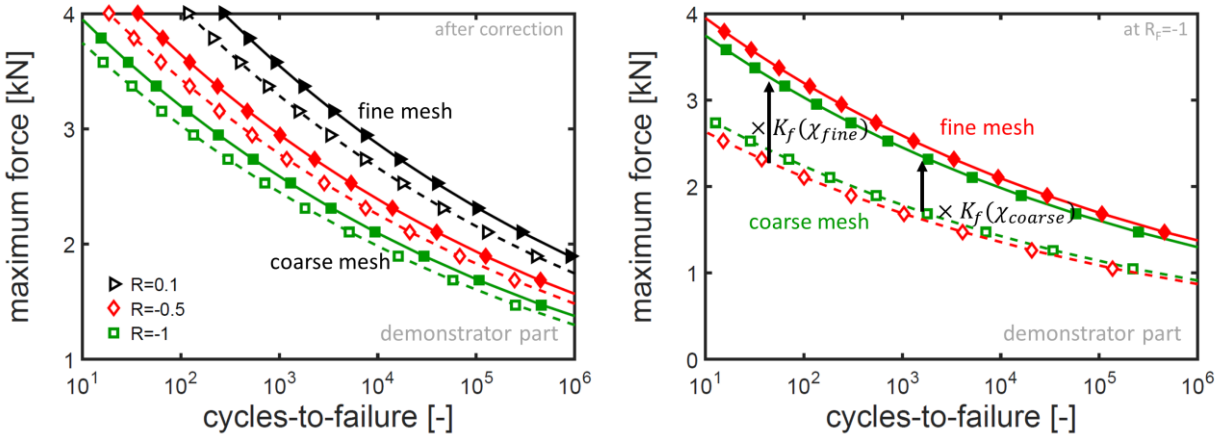

Figure 15: Predicted FN curves for the demonstrator part with fine mesh and a coarser mesh. (a) For various load ratios after correction for the stress gradient, where the solid line and closed markers represent the fine mesh and the dashed line and open markers the coarser mesh. (b) For R_F=-1 before (open markers) and after correction (closed markers) for the fine mesh (diamonds) and the coarse mesh (squares).

Summary and Next Steps

This work presents a systematic framework that enables accurate lifetime predictions on injection molded parts. When step-by-step adding complexity, a consistent framework, valid for a large range of load ratios, microstructures, and stress concentrations, allows predictions on part level with an accuracy of a factor 5-30 on lifetime.

Improvement of the method to correct for stress concentrations is a topic of further investigation and the plasticity correction methods are being explored. In addition, also more validation data is generated on an additional demonstrator part, the influence of environmental conditions (temperature and humidity) will be studied, and more materials are being characterized.

The framework highlighted in this paper is now ready and available in Digimat including two material cards of DSM Engineering Plastics grades. The enhanced model will correct for anisotropy, local stress ratio, and stress gradients and can be evaluated with the Digimat RP fatigue post-processer.

Bibliography

1. M. Weiss V. Tuncay, S. Richter, J. Broz, Umfassende Simulation und vernetzte Intelligenz im Thermomanagement. MTZ - Motortechnische Zeitschrift, 2017, Volume 78, Issue 9, pp 42–49
2. D. Winter, Survey: CAFE Rules Likely to Get Tougher, Not Easier, 2016, WardsAuto
3. D. Winter, Auto Engineers See Future CAFE Rules Easing, 2017, WardsAuto
4. Elringklinger, Lightweight plastic components. For cars and commercial vehicles. Brochure, 2017.
5. U.W. Gedde, J. Viebke, H. Leijström, M. Ifwarson, Long-term properties of hot-water polyolefin pipes - a review, Polym. Eng. Sci. 34 (24) (1994) 1773-1787.
6. R.W. Lang, A. Stern, G. Doerner, Applicability and limitations of current lifetime prediction models for thermoplastics pipes under internal pressure, Die Angew, Makromol. Chem. 247 (1) (1997) 131-

145.

7. R.P.M. Janssen, L.E. Govaert, H.E.H. Meijer, An analytical method to predict fatigue life of thermoplastics in uniaxial loading: sensitivity to wave type, frequency, and stress amplitude, Macromolecules 41 (7) (2008) 2531-2540.
8. M.J.W. Kanters, T. Kurokawa, L.E. Govaert, Competition between plasticity-controlled and crack-growth controlled failure in static and cyclic fatigue of thermoplastic polymer systems. Polymer Testing 50 (2016) 101-110
9. M.J.W. Kanters, T.A.P. Engels, T.B. van Erp, L.E. Govaert, Predicting long-term crack growth dominated static fatigue based on short-term cyclic testing, International Journal of Fatigue 12 (2018) 318–327.
10. M. De Monte, E. Moosbrugger, M. Quaresimin, Influence of temperature and thickness on the off-axis behaviour of short glass fibre reinforced polyamide 6.6 – Quasi-static loading, Composites: Part A 41 (2010) 859–871.
11. e-Xstream engineering, "Digimat documentation Release 2019.0," 2019, http://www.e-xstream.com/
12. C.M. Sonsino, E. Moosbrugger, Fatigue design of highly loaded short-glass-fibre reinforced polyamide parts in engine compartments, International Journal of Fatigue 30 (2008) 1279–1288.
13. S. Mortazavian, A. Fatemi, Effects of mean stress and stress concentration on fatigue behavior of short fiber reinforced polymer composites, Fatigue Fract. Engng. Mater. Struct., 2016, 39, 149–166.
14. A. Primetzhofer, G. Stadler, G. Pinter, F. Grün, Lifetime assessment of anisotropic materials by the example short fibre reinforced plastic, International Journal of Fatigue 120 (2019) 294–302.
15. L., Susmel, The theory of critical distances: a review of its applications in fatigue. Engineering Fracture Mechanics, 75, (2008), 1706-1724.
16. H. Neuber, Theory of Stress Concentration for Shear-Strained Prismatical Bodies With Arbitrary Nonlinear Stress-Strain Law, J. Appl. Mech., 28, (1961), 544.
17. K. Molski and G. Glinka, Method of Elastic-Plastic Stress and Strain Calculation at a Notch Root, Materials Science and Engineering, 50 (1981) 93 – 100.